Title
Experimental and theoretical studies of the interaction of gas phase nitric acid and water with a self-assembled monolayer

Journal
Physical Chemistry Chemical Physics, 15(2)

ISSN
1463-9076 1463-9084

Authors
Moussa, S. G
Stern, A. C
Raff, J. D
et al.

Publication Date
2013

DOI
10.1039/c2cp42405c

Peer reviewed

PCCP

Physical Chemistry Chemical Physics

www.rsc.org/pccp

Volume 15 | Number 2 | 14 January 2013 | Pages 381–704

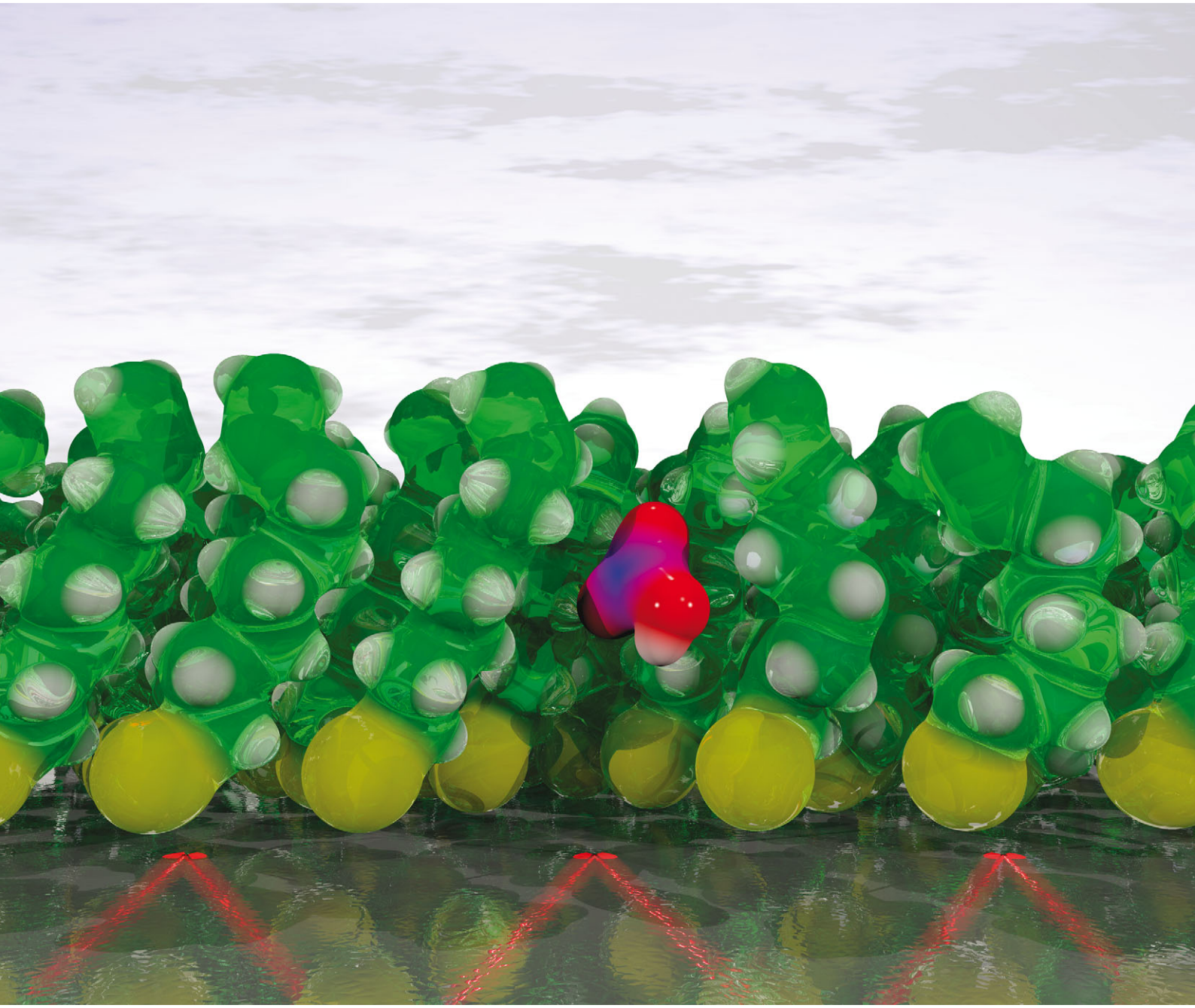

ISSN 1463-9076

PAPER

D. J. Tobias, B. J. Finlayson-Pitts *et al.*

Experimental and theoretical studies of the interaction of gas phase nitric acid and water with a self-assembled monolayer

1463-9076(2013)15:2;1-K

PCCP

RSC Publishing

PAPER

View Article Online
View Journal | View Issue

Cite this: *Phys. Chem. Chem. Phys.*, 2013, **15**, 448

Experimental and theoretical studies of the interaction of gas phase nitric acid and water with a self-assembled monolayer

S. G. Moussa, A. C. Stern, J. D. Raff,† C. W. Dilbeck, D. J. Tobias* and B. J. Finlayson-Pitts*

Received 15th July 2012,
Accepted 1st November 2012

DOI: 10.1039/c2cp42405c

www.rsc.org/pccp

Nitric acid in air is formed by atmospheric reactions of oxides of nitrogen and is removed primarily through deposition to surfaces, either as the gas or after conversion to particulate nitrate. Many of the surfaces and particles have organic coatings, but relatively little is known about the interaction of nitric acid with organic films. We report here studies of the interaction of gaseous HNO_3 with a self-assembled monolayer (SAM) formed by reacting 7-octenyltrichlorosilane [$H_2C{=}CH(CH_2)_6SiCl_3$] with the surface of a germanium infrared-transmitting attenuated total reflectance (ATR) crystal that was coated with a thin layer of silicon oxide (SiO_x). The SAM was exposed at 298 ± 2 K to dry HNO_3 in a flow of N_2, followed by HNO_3 in humid N_2 at a controlled relative humidity (RH) between 20–90%. For comparison, similar studies were carried out using a similar crystal without the SAM coating. Changes in the surface were followed using Fourier transform infared spectroscopy (FTIR). In the case of the SAM-coated crystal, molecular HNO_3 and smaller amounts of NO_3^- ions were observed on the surface upon exposure to dry HNO_3. Addition of water vapor led to less molecular HNO_3 and more H_3O^+ and NO_3^- complexed to water, but surprisingly, molecular HNO_3 was still evident in the spectra up to 70% RH. This suggests that part of the HNO_3 observed was initially trapped in pockets within the SAM and shielded from water vapor. After increasing the RH to 90% and then exposing the film to a flow of dry N_2, molecular nitric acid was regenerated, as expected from recombination of protons and nitrate ions as water evaporated. The nitric acid ultimately evaporated from the film. On the other hand, exposure of the SAM to HNO_3 and H_2O simultaneously gave only hydronium and nitrate ions. Molecular dynamics simulations of defective SAMs in the presence of HNO_3 and water predict that nitric acid intercalates in defects as a complex with a single water molecule that is protected by alkyl chains from interacting with additional water molecules. These studies are consistent with the recently proposed hydrophobic nature of HNO_3. Under atmospheric conditions, if HNO_3 is formed in organic layers on surfaces in the boundary layer, *e.g.* through NO_3 or N_2O_5 reactions, it may exist to a significant extent in its molecular form rather than fully dissociated to nitrate ions.

Introduction

Nitric acid is considered to be the end-product of oxidation of oxides of nitrogen in the atmosphere.[1] This acid reacts with ammonia and amines to form solid or aqueous phase nitrate particles, and can also be taken up into other types of atmospheric particles. Removal of gaseous HNO_3 and particulate nitrates takes place primarily through wet and dry deposition, in what were once considered to be terminal removal processes. However, there are now a number of laboratory and field studies that suggest that nitric acid can be converted back into gaseous oxides of nitrogen such as NO, NO_2 and HONO.[2–8]

Nitric acid is a strong acid, but it requires a cluster of at least four water molecules to dissociate in the gas phase.[9–11] In bulk aqueous solutions and on ice, nitric acid can form hydrates with 1, 2 or 3 water molecules, depending on the concentration.[12–24] Such hydrates, as well as the HNO_3 dimer, have also been seen on solid surfaces during the hydrolysis of NO_2 at

Department of Chemistry, University of California, Irvine, CA 92697-2025, USA. E-mail: bjfinlay@uci.edu(for experiments), dtobias@uci.edu, (for theory); Fax: +1 949 824-2420; Tel: +1 949 824-7670, +1 949 824-4295

† Current address: School of Public & Environmental Affairs and Department of Chemistry, Indiana University, Bloomington, IN 47405-2204.

50% relative humidity.[25] Both theory and experiment suggest that nitric acid is not fully dissociated at the interface of aqueous solutions.[26–34] Indeed, recent results suggest that undissociated HNO_3 interacts very weakly with water.[33,34]

Because of the presence of significant concentrations of water vapor in the lower atmosphere, there is an abundance of water available on surfaces such as roads, buildings, *etc.*, as well as in airborne particles.[35–37] Surfaces in the tropospheric boundary layer also hold a variety of adsorbed organic compounds.[38–42] However, there are relatively few studies of the interactions of HNO_3 with such surface-bound organics. Shultz and coworkers[43] showed that HNO_3 in CCl_4 was undissociated, while Donaldson and coworkers[4] have shown that HNO_3 adsorbed into an organic film could photodissociate to generate gas phase NO_2 and/or HONO. In this case, the organic acted as a photosensitizer.

The goal of this study is to understand the interaction of HNO_3 with a relatively well-characterized organic film, and the effect of water on these interactions using attenuated total reflectance Fourier transform infrared spectroscopy (ATR-FTIR).[44] Self-assembled monolayers (SAMs) are used as a model for organic compounds that are adsorbed on atmospheric surfaces.[45–53] We show, *via* a combination of experimental spectroscopic data and molecular dynamics simulations, that some of the gas phase HNO_3 intercalates between the hydrocarbon chains and is not fully available to interact with water that is added subsequently. However, simultaneous exposure of the SAM to HNO_3 and H_2O only generates protons and nitrate ions. These studies suggest that if nitric acid is formed in an organic matrix, for example on boundary layer surfaces, it may exist in an undissociated molecular form whose chemistry and photochemistry is different than that of the nitrate ion formed upon dissociation.

Experimental

Preparation of ATR crystals

A germanium attenuated total reflectance (ATR) crystal (Pike Technologies, 80 mm × 10 mm × 4 mm) allowing for 10 reflections along the length of the crystal was used both as a substrate and as an optical element with which to detect adsorbed H_2O, HNO_3, NO_3^-, and the attached SAMs. While well-ordered SAMs are readily synthesized on silica,[54–58] SiO_x does not transmit below 1500 cm^{-1}, a region where both nitric acid and nitrate ions have strong absorptions that are readily followed experimentally. As a result, a germanium ATR crystal coated with a thin layer of SiO_x was used for these studies, which extended the IR window down to 860 cm^{-1}. The Ge crystal had a thin layer of SiO_x (average of 20 nm based on ellipsometry measurements) on its surface that was deposited using plasma-enhanced chemical vapor deposition (PECVD). The SiO_2 was generated by the oxidation of SiH_4 (2.75 mL min^{-1}) with N_2O (50 mL min^{-1}) in the presence of nitrogen. Prior to use and derivatization, ATR crystals were rinsed with double distilled water (Milli-Q Plus, 18.2 MΩ cm), dried with nitrogen (Oxygen Service Co., UHP, 99.999%) and placed in an argon plasma discharge cleaner (Harrick Scientific Plasma Cleaner/Sterilizer PDC-32G, medium power) for ~10 min to remove organic contaminants. The SAM, designated hereafter as C8=, was formed by reacting the SiO_x-coated ATR crystals with 7-octenyltrichlorosilane. [$H_2C{=}CH(CH_2)_6SiCl_3$] (Sigma-Aldrich, mixture of isomers, 96%). A detailed description of the procedure for depositing the SAMs onto the ATR crystal has been described previously.[45,46,59,60]

Exposure of surfaces to HNO_3 and H_2O

The ATR crystal was placed in a horizontal flow-through cell (Pike Technologies) with a head space of ~500 μL,[60] where it was purged overnight with a dry stream of N_2 inside the sample compartment of a Mattson Galaxy 5020 FTIR spectrometer. The stainless steel parts of the ATR cell were coated with halocarbon wax, and Teflon tubing and connections were used to minimize loss of HNO_3 on the sampling lines and walls of the cell. For the 4000–850 cm^{-1} region, the depth of penetration of the evanescent wave from the Ge ATR crystal into air was calculated to be 0.13–0.61 μm, much greater than the thickness of the combined SAM (~1.3 nm) and SiO_x layer (~20 nm). The infrared beam thus interrogates the entire organic monolayer and provides spectra similar to a transmission spectrum. All ATR measurements were taken at a total pressure of 1 atm. Single beam spectra were collected over the spectral range 4000–600 cm^{-1}. For each experiment, a total of 128 scans were collected at 4 cm^{-1} resolution.

Dry gaseous HNO_3 was generated by flowing N_2 (20 mL min^{-1}) over the surface of a solution of HNO_3/H_2SO_4 (1 : 3 v/v) in a glass trap (69.7 wt% HNO_3, Fisher; 96.0 wt% H_2SO_4, Fisher). The flow of HNO_3 was further combined and diluted with a flow of dry or humid nitrogen with known relative humidity, making the total flow ~220 mL min^{-1}. A portion, (70–74 mL min^{-1}) of this total flow, was diverted to the ATR cell. The concentration of HNO_3 over the ATR crystal after dilution was 1.7×10^{16} molecules cm^{-3} (~700 ppm). Desired water vapor concentrations (relative humidity) were achieved by mixing measured flows of dry and humid N_2 gas. Humid N_2 flows were obtained by bubbling dry nitrogen through water in two borosilicate fritted glass bubblers in a thermostated water bath. The temperatures of the spectrometer, cell, and water bath and the trap containing the HNO_3 were kept constant at 298 ± 2 K as measured by a thermocouple (OMEGA HH506).[37,59] For some experiments, the SAM was exposed simultaneously to HNO_3 and H_2O at 50% RH by redirecting the flow of N_2 to pass over the headspace of a 5 M aqueous solution of HNO_3. The HNO_3 concentration in the gas phase in these experiments was calculated to be 1.7×10^{13} molecule cm^{-3} (~700 ppb) based on known H_2O–HNO_3 equilibria.[61,62]

Scanning electron microscopy (SEM)

SEM images were collected on a Zeiss Ultra 55 field emission scanning electron microscope using an in-column energy selective backscattered electron detector. An accelerating voltage of 2000 V was used, and a bias of −1500 V was applied to the collector grid to eliminate secondary electrons and low-energy

backscattered electrons. The images therefore are produced only by backscattered electrons. A working distance of 3.9 mm was used.

Molecular dynamics (MD) simulations

To shed light on the experimental findings, simulations were performed using a self-assembled monolayer composed of 64 eight-carbon, vinyl-terminated alkylthiolates (1-octenethiolate) chemically adsorbed on a gold (111) lattice coexisting with humid HNO_3 vapor. As in our previous work,[45,59] the choice of alkylthiolates on gold in computer simulations rather than alkylsilanes on germanium silicate glass substrate as in the experiment was driven by methodological considerations. While potentials for accurately describing the interactions between alkanethiolates and the gold(111) surface are well established,[63] the relatively complex bonding between alkylsiloxanes and silicon oxide surfaces introduces uncertainties in the development of atomistic models for alkylsiloxane SAMs.[64] Moreover, it has been shown that the structural differences between SAMs composed of long alkane chains on silica and on gold are minor.[65–67]

Chemisorption of the alkylthiolates to the gold surface was modeled using a two-dimensional corrugation potential in conjunction with a Lennard-Jones 9–6 potential acting along the vector normal to the SAM surface. The alkylthiolate, gold, and corrugation force field parameters used were those employed successfully in several previous studies.[63,68] The van der Waals interactions of HNO_3 were modeled using the Lennard-Jones parameters of the Amber generalized force field,[69] while the electrostatic interactions were accounted for with atom-centered point charges fit to the electrostatic potential of HNO_3.[69] All intramolecular degrees of freedom within an HNO_3 molecule were held rigid using high force constants for motions associated with planarity, bending, and stretching, with the sole exception of the torsional potential involving the proton, which was modeled as a cosine with a barrier height of 2.86 kcal mol^{-1} and a periodicity of two. Water molecules were modeled using the rigid TIP3P parameters.[70]

The silica surface that results from the PECVD process is amorphous and rough on the molecular scale. By extension, it can be safely assumed that the SAM coating will be far more disordered than an atomically smooth alkylthiolate SAM. Although it was impractical to consider all possible arrangements of SAM defects, the goal of this study was more modest: to simulate one example of a defective monolayer to investigate the possibility that HNO_3 may be able to intercalate between the hydrocarbon chains of the monolayer and remain buried and protected from water vapor. To introduce defects in the monolayer surface, four SAM molecules were removed. Fig. 1 shows the sites of the defects denoted by X's that were used in the MD simulations. After equilibrating the monolayer, a single HNO_3 was added to the simulation cell and simulated until the HNO_3 settled into a defect, at which point the simulation was then continued with between 0 and 8 added water molecules. Canonical ensemble simulations (constant particle number, volume, and temperature) were performed at a temperature of 300 K maintained by running Langevin dynamics with a damping coefficient of 1 ps^{-1}. A reversible, multiple timestep algorithm[71] was used to integrate the equations of motion with time steps of 2 fs for the electrostatic forces and short-ranged nonbonded forces, and 1 fs for the bonded forces. The smooth particle mesh Ewald method[72] was used to calculate the electrostatic interactions. The short-ranged, real space interactions were cut off at 11 Å using a switching function. Simulations were conducted using the NAMD software package.[73]

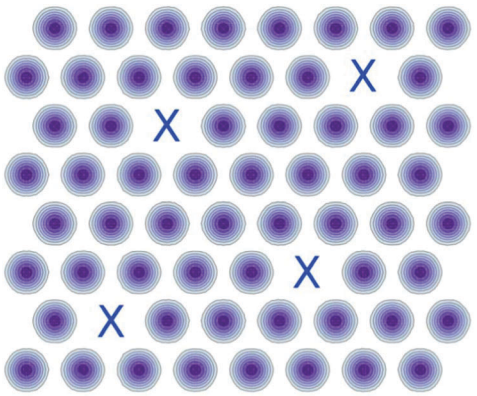

Fig. 1 Two dimensional contour plots viewed from the top of the corrugation potential that acts on the sulfur atoms of the alkylthiols. The lattice sites corresponding to the defects are marked by an ''X''.

Results and discussion

A. Interaction of gaseous HNO_3 and water vapor with a bare SiO_x/Ge surface

Fig. 2 shows the absorbance spectrum (red trace) obtained when dry gaseous nitric acid flows over the SiO_x/Ge ATR crystal. Absorbance is defined here as $\log(S_0/S_1)$ where S_0 is the single beam spectrum of the crystal prior to addition of HNO_3 and S_1 is the single beam spectrum after exposure to HNO_3. Thus, positive peaks signify new species on the crystal due to uptake and reactions of HNO_3. Three distinct peaks appear. Those at 1673 cm^{-1} and 1303 cm^{-1} are assigned to well known ν_2 (NO_2 antisymmetric stretch) and ν_4 (NO_2 symmetric stretch) vibrational modes of HNO_3, which have been reported for HNO_3 in aqueous solutions,[26,74,75] in the gas phase[76,77] and on ice.[23,24,78,79] The peak at 1265 cm^{-1} is assigned to the nitrite ion,[80] and indicates that the uptake of HNO_3 onto the crystal is accompanied by a surface reaction that forms NO_2^-. Underwood *et al.* also observed the presence of nitrite ion on mineral oxide surfaces at $\sim$1250 cm^{-1}.[81]

The bare SiO_x/Ge surface continued to take up nitric acid for approximately two hours, at which time peaks due to molecular HNO_3 no longer changed in intensity. Once equilibrium was established, a flow of N_2 containing various amounts of water vapor that increased in stepwise fashion from 20 to 90% RH was then added to the HNO_3 flow. The concentration of HNO_3 above the crystal was held constant to minimize evaporation of nitric acid from the surface. New peaks appear around 3400 cm^{-1} and 1641 cm^{-1} with a shoulder at 1708 cm^{-1}. A broad feature in

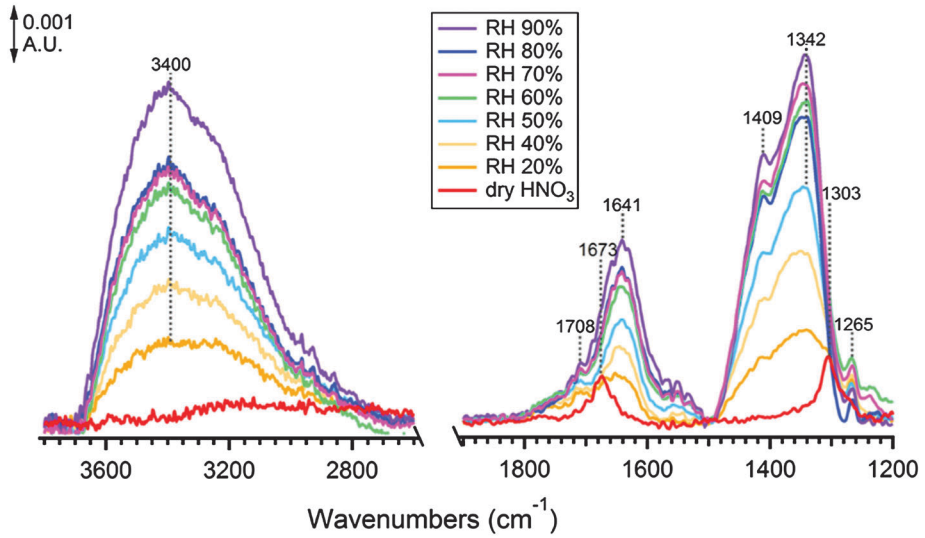

Fig. 2 Infrared spectra of a SiO_x/Ge ATR crystal after exposure to dry HNO_3 (1.7×10^{16} molecule cm^{-3}) followed by the addition of water vapor to the flow to give 20–90% RH at 298 K. The *y*-axis is $\log(S_0/S_1)$ where S_0 is the single beam spectrum of a SiO_x/Ge ATR crystal prior to exposure to HNO_3 or H_2O and S_1 is the single beam spectrum of the same SiO_x/Ge ATR crystal after exposure to HNO_3 before and then after addition of H_2O.

the 1300–1500 cm^{-1} region also appears. The peaks due to molecular HNO_3 at 1673 and 1303 cm^{-1} are strongly overlapped by the new product peaks, and become essentially undetectable when water vapor is added. The peak at 1708 cm^{-1} is assigned to H_3O^+.[23,82] Mashburn *et al.*[83] and Baltrusaitis *et al.*[84] similarly assigned peaks in this region to H_3O^+ on clays and aluminum oxide surfaces. Those centered at 3400 and 1641 cm^{-1} are assigned to the stretching and bending modes of H_2O, respectively, where water may be complexed in part to nitrate ions.[24,85–87] The peaks in the 1300–1500 cm^{-1} region are due to nitrate ions complexed to water. As discussed in detail elsewhere,[24,87] the antisymmetric stretching vibration (ν_3) of NO_3^- is degenerate for the planar structure, but the degeneracy is removed and two bands appear if the symmetry is changed by interaction with other species such as solvent molecules or a surface.[88] At 90% relative humidity, the splitting in the ν_3 mode is 67 cm^{-1}, which is typical of NO_3^- bound to approximately five water molecules.[24,87]

It is well known that HNO_3 readily adsorbs to silica.[89,90] However, SEM micrographs of the crystal surface (not shown) revealed that the SiO_x coating was not uniform, leaving regions of exposed germanium. Nitric acid is known to oxidize Ge.[91–93] This forms the metal oxide and reduced nitrogen oxides such as NO_2/N_2O_4 and NO_2^- *via* thermodynamically favored net reactions such as:

$$Ge + 2NO_3^- \rightarrow GeO_2 + 2NO_2^- \quad (1)$$

$$Ge + 4NO_3^- + 4H^+ \rightarrow GeO_2 + 2N_2O_4 \text{ (or } 4NO_2) + 2H_2O \quad (2)$$

Thus, the spectra in Fig. 2 are consistent with a reaction of HNO_3 with the uncoated germanium to form NO_2^-. This remains on the surface, as does HNO_3 which, upon the addition of water, dissociates to H_3O^+ and NO_3^-. The spectra in the nitrate ion region are very similar to those reported for nitrate ions on metal oxide surfaces and clays.[83,84,90] Gaseous products such as NO_2/N_2O_4 would be removed in the gas stream, and likely also undergo some hydrolysis in the water film to form $HONO/NO_2^-$ and HNO_3/NO_3^-.[94]

Fig. 3 shows the sequence of spectra when the flow of the gaseous HNO_3–H_2O mixture is replaced by a flow of dry N_2. The peaks due to water at 1641 cm^{-1} and ~3400 cm^{-1} decrease as the surface dries out, but there are no other significant changes in the spectrum. This indicates that water evaporates during the drying process, leaving nitrate and nitrite ions behind on the surface, along with residual water.

B. Interaction of gaseous HNO_3 and water vapor with a self-assembled monolayer on SiO_x/Ge

Fig. 4 shows spectra similar to those in Fig. 2 but for a C8= SAM coated SiO_x/Ge crystal exposed first to dry HNO_3 then to humidified N_2 at various RH. Organic trichlorosilanes form SAMs on both silica surfaces and on germanium,[54,60] although those on Ge are less stable.[54,60,95–101] Nevertheless, SAMs are expected to cover the entire surface. Given the presence of the double bond in the SAM, the irregular SiO_x coating of the Ge, and the instability of the SAM on Ge, some disorder is expected in the film. This will be reflected in the peak positions and widths.[54,55,102,103] The antisymmetric $-CH_2-$ stretch in a well-ordered SAM has a peak position at 2917 cm^{-1} and a full width at half-maximum (fwhm) of 14–16 cm^{-1}.[55] For the C8= SAM on borosilicate glass,[59] the peak is at 2919 with a fwhm of 21 cm^{-1}. For the C8= SAM on a germanium ATR crystal,[60] the peak is at 2924 with a fwhm of 30 cm^{-1}. In the present case of SiO_x/Ge, the peak is at 2920 cm^{-1}, with a fwhm of 23–25 cm^{-1}.

There are a number of significant differences between experiments conducted in the presence of a SAM coating compared to those on bare Ge–SiO_x surfaces. For example, the time required for HNO_3 to reach equilibrium with the surface was much shorter than for the bare crystal (~10–15 min compared to several hours),

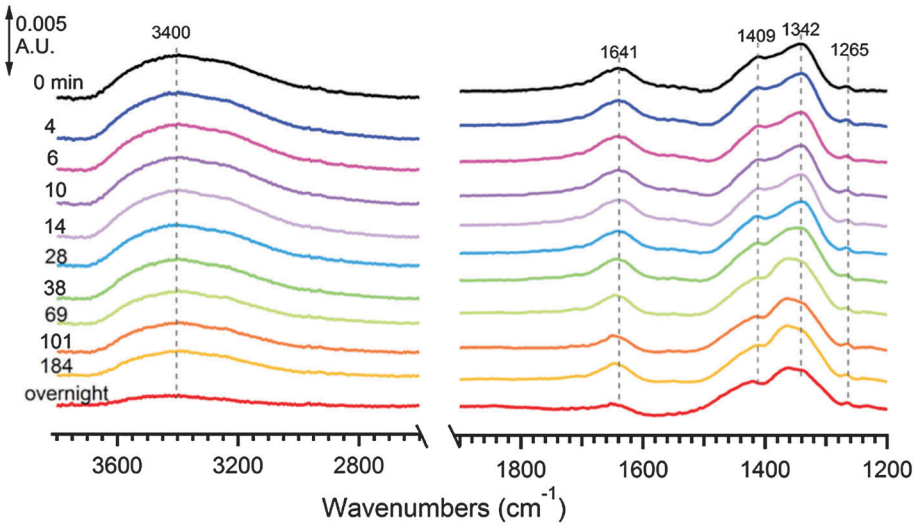

Fig. 3 Infrared spectra of a SiO_x/Ge ATR crystal exposed to HNO_3 and H_2O, and then to dry N_2 for the times shown. The *y*-axis is $\log(S_0/S_1)$ where S_0 is the single beam spectrum of the SiO_x/Ge ATR crystal prior to exposure to HNO_3 and H_2O and S_1 is the single beam spectrum after exposure to HNO_3 and H_2O, and then to dry N_2 for the times shown.

and a peak due to NO_2^- was not observed. The longer time needed for the adsorbed nitric acid to stabilize on the bare crystal reflects the time required to first convert the germanium to its oxide, and then to saturate the surface with HNO_3. For the SAM-coated crystal, HNO_3 is not reacting directly with Ge on the underlying crystal surface, suggesting that the SAM coverage is relatively complete and blocks these sites. It should be noted, however, that exposure of the SAM-coated crystal to water vapor alone resulted in a negative peak due to the surface free O–H stretch at 3695 cm^{-1}. This indicates that the smaller water molecule can still access some of the crystal surface (data not shown).

Exposure to dry HNO_3 produces a broad shoulder in the 1300–1500 cm^{-1} region where the ν_3 antisymmetric stretching mode of NO_3^- occurs. There are two possible sources of NO_3^- in the dry system: dissociation of HNO_3 or its self-reaction/autoionization to form $NO_3^- + NO_2^+ + H_2O$. Traces of water will be present in this system which can promote some dissociation of HNO_3. Autoionization generates NO_2^+ which has an infrared absorption band[94] at ~2300 cm^{-1}, but it is sufficiently weak that it may not be detectable under the present conditions. The NO_2^+ ion reacts with two molecules of water to regenerate $HNO_3 + H_3O^+$, so the net effect of these two possibilities is similar when water vapor is added.

The shoulder attributed to NO_3^- is structureless and centered at ~1395 cm^{-1} for RH below 50%. This is in contrast to that in the absence of the SAM (Fig. 2) where two bands due to splitting of the degeneracy are detectable even at 20% RH and the maximum peak absorbance is at 1342 cm^{-1}. This suggests there is an additional underlying peak in this region for the SAM-coated crystal. In order to probe this, a fraction (0.30) of the spectrum at 90% RH was subtracted from that at the 0% RH spectrum, in order to compensate for the contribution due to the nitrate ion. As seen by the black line shown below the original data in Fig. 4, a small peak at 1395 cm^{-1} emerges from this subtraction. This is attributed to the HON bend of HNO_3 which is also observed in the liquid[74] and at anhydrous interfaces.[26] This peak is not obvious in the absence of the SAM, suggesting that the interaction of the HNO_3 with the SiO_x/Ge surface is different. A strong interaction with the surface in the absence of the SAM *via* the hydrogen and nitrogen may shift and broaden the HON absorption to the point that it is not evident in the spectrum.

The peak at 1301 cm^{-1} due to molecular HNO_3 is detectable up to 70% RH in the presence of the SAM (Fig. 4 inset), whereas it was not detectable on the bare crystal after exposure to water vapor, even at 20% RH. Based on previous studies[25] where HNO_3 was formed on surfaces in the presence of water vapor *via* the hydrolysis of NO_2, it seems likely that some of the nitric acid is present in the form of hydrates. Such hydrates may contribute to the peak at 1637 cm^{-1} (Fig. 4), since complexation of HNO_3 with water is expected to red-shift the antisymmetric NO_2 stretch in the acid by ~10 cm^{-1}.[24,26,86,104] The O–H stretching absorptions due to nitric acid–water complexes (2975 cm^{-1} and 2812 cm^{-1}) are also expected to shift relative to anhydrous nitric acid,[24,25] but they are overwhelmed by the large contribution due to water in this region. However, regardless of a potential contribution of nitric acid hydrates to the spectra, it is clear that the SAM coating inhibits reaction of HNO_3 with the Ge substrate as well as the dissociation of HNO_3 on the surface in the presence of water vapor compared to the bare SiO_x/Ge surface.

The intensities of both the nitrate and water peaks on the SAM-coated crystal are significantly smaller, by about a factor of two, than those for the bare crystal. This is not surprising since the uptake of water would be expected to be greater on a bare oxide crystal than on a surface that is largely covered with a hydrophobic organic layer. The presence of large amounts of water would promote more dissociation of HNO_3.

It is clear from the spectra in Fig. 4 that the amount of molecular HNO_3 relative to nitrate ions decreases as the relative

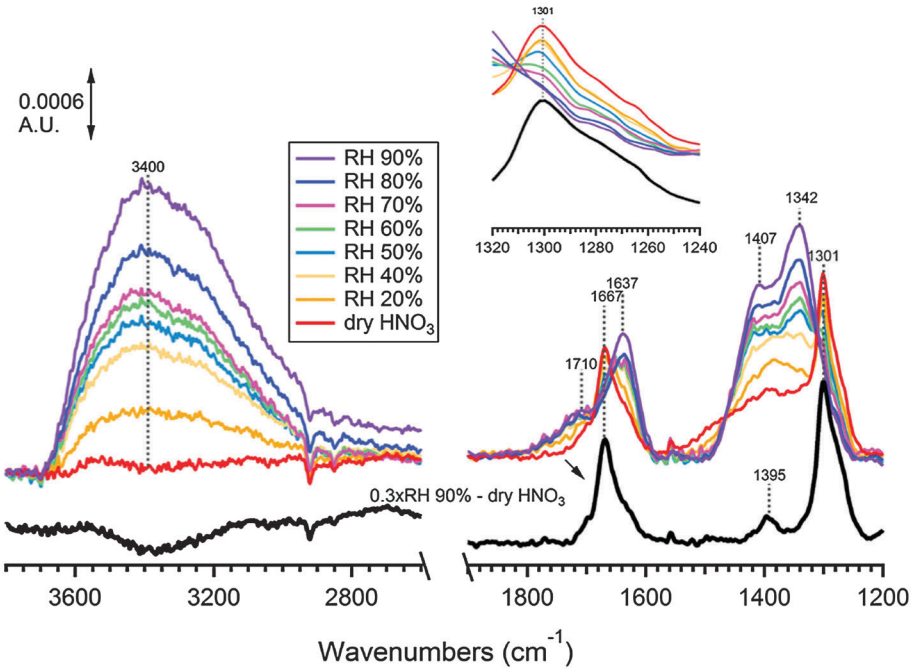

Fig. 4 Infrared spectra of a C8= SAM-coated SiO_x/Ge crystal after exposure to dry HNO_3 followed by water vapor at different RH at 298 K. The *y*-axis is $\log(S_0/S_1)$ where S_0 is the single beam spectrum of the C8= SAM on a SiO_x/Ge ATR crystal prior to exposure to HNO_3 or H_2O and S_1 is the single beam spectrum of the C8= SAM after exposure to HNO_3 or H_2O. The dark black trace is the spectrum resulting from the subtraction of 0.3× the 90% RH spectrum from that for dry HNO_3. The inset expands the region around 1301 cm^{-1}.

humidity increases, as expected for water-promoted dissociation of the acid. If the transition intensities of the surface species were the same as for the gas phase, a rough estimate of the relative amounts of HNO_3 and NO_3^- can be made as follows. The theoretical infrared intensity of the NO_2/NO_3 symmetric stretch of HNO_3 (at 1301 cm^{-1} in the present studies) using MP2 TZ2P and assuming harmonicity was reported to be 206 km mol^{-1}.[105] The theoretical intensities (anharmonic) for the nitrate ion are 845 km mol^{-1} for nitrate coordinated to one water molecule and an average of 592 km mol^{-1} for nitrate coordinated to 4–5 water molecules.[25] The spectra in the 1200–1500 cm^{-1} region in Fig. 4 were separated into two overlapping contributions, one from HNO_3 centered at 1301 cm^{-1} and a broader contribution from NO_3^-. Using the peak areas of the two, HNO_3 is 1.6 times greater than NO_3^- in the "dry" case. At 50% RH when it was assumed that NO_3^- is coordinated to 4–5 water molecules but HNO_3 is not complexed to water, the HNO_3 would be present at 30% of the nitrate ion concentration. However, calculations by Staikova and Donaldson[104] suggest that the theoretical intensity of the molecule HNO_3 band could increase by a factor of five when complexed to one water. If this were the case for HNO_3 at 50% RH, then the HNO_3 would be present at only 6% of the nitrate ions. These estimates should be taken as order-of-magnitude, given the use of theoretical intensities for gas phase species, the uncertainty in the number of water molecules complexed to HNO_3 and NO_3^-, and the use of a mixture of harmonic and anharmonic calculations.

Fig. 5 shows the sequence of spectra obtained when the flow of the gaseous HNO_3–H_2O mixture is replaced by a flow of dry N_2 on the SAM-coated crystal. In contrast to the case of the bare crystal, peaks at 1667 and 1301 cm^{-1} assigned to molecular HNO_3 appear shortly after drying is initiated. Their relative intensities increase and then decrease over the course of three hours. They completely disappear after drying overnight. This indicates that nitrate ions and protons must be in sufficiently close proximity that they can recombine while water is evaporating and the aqueous thin film becomes more concentrated. Recombination leads to molecular HNO_3, which desorbs into the gas phase and is removed in the gas stream.

The following model is consistent with these data. On the bare crystal, dry nitric acid oxidizes exposed Ge in the portions of the crystal that were not coated with SiO_x. This converts Ge to its oxide and simultaneously generates reduced forms of oxides of nitrogen such as NO_2^-, which remains on the surface (1265 cm^{-1} peak, Fig. 2), and N_2O_4/NO_2, which will desorb into the gas stream. Once the surface has been completely oxidized, molecular HNO_3 physisorbs (1673 and 1303 cm^{-1}, Fig. 2). The subsequent addition of water leads to dissociation of surface-adsorbed HNO_3 so that the degenerate bands due to NO_3^- complexed to water then appear on the surface in the 1300–1500 cm^{-1} range (Fig. 2). Interaction of the proton and NO_3^- with the ionic oxide surface is sufficiently strong so that replacement of the HNO_3/H_2O with dry N_2 simply leads to removal of much of the water. This leaves nitrate ions bound to Ge^{4+} on the surface (Fig. 3).

When most of the surface is initially covered with the hydrophobic SAM, the SiO_x/Ge crystal is largely protected from exposure to nitric acid. As a result, the equilibrium between

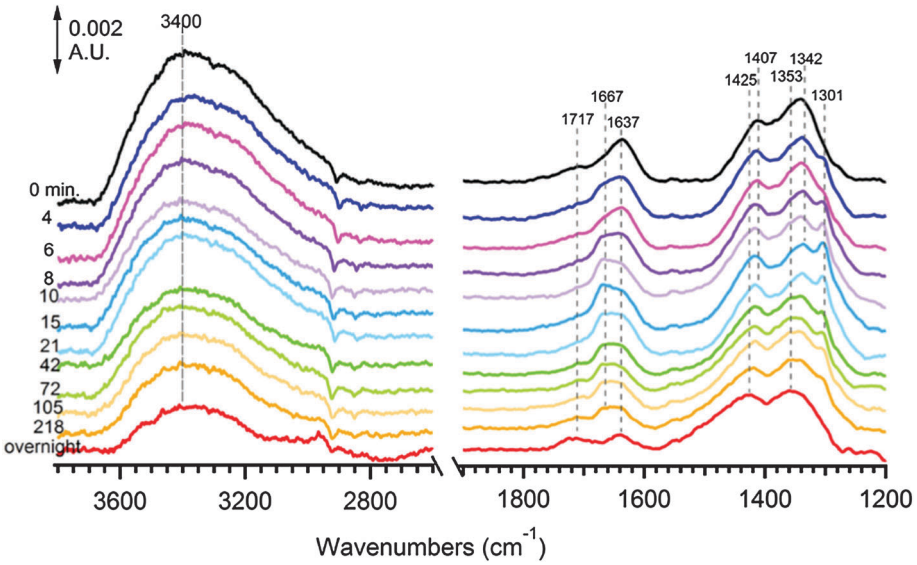

Fig. 5 Infrared spectra of C8= SAM on SiO_x/Ge ATR crystal exposed to HNO_3 and H_2O then to dry N_2 for the times shown. The *y*-axis is $\log(S_0/S_1)$ where S_0 is the single beam spectrum of a dry C8= SAM on a SiO_x/Ge ATR crystal prior to exposure to HNO_3 and H_2O and S_1 is the single beam spectrum of C8= exposed to HNO_3 and H_2O, and then to dry N_2 for the times shown.

physisorbed HNO_3 and the gas phase is reached much faster and the formation of nitrite ions that accompanies oxidation of Ge on the crystal is not observed. Interestingly, the amount of molecular HNO_3 on the dry SAM-coated surface based on the 1301 cm^{-1} peak is about double that on the bare crystal (Fig. 2 *vs.* Fig. 4) and NO_3^- is observed immediately (peak at 1395 cm^{-1}), even in the absence of water.

We propose that HNO_3 intercalates between the chains of the SAM, perhaps in pores created due to the disorder in the monolayer. The formation of nitrate ions in the absence of water could reflect a high local concentration of HNO_3 in the pores, leading to autoionization to $NO_2^+NO_3^-$ and the generation of nitrate ions as discussed earlier. This "trapped HNO_3" is not readily accessible to added water, leading to less dissociation as the RH is increased. Consistent with this model is the persistence of the bands due to molecular HNO_3 up to at least 70% RH (Fig. 4). When dissociation does occur within these pores or between chains at high RH, the proton and NO_3^- will be in relatively close proximity, so that subsequent drying allows them to readily recombine to form molecular HNO_3 which eventually evaporates as shown in (Fig. 5). This mechanism is summarized schematically in Fig. 6.

Support for this hypothesis is found in the impact of HNO_3 on the order/disorder of the monolayer. Decreases in the intensity of C–H stretching vibrations for the SAM in the 2800–3000 cm^{-1} region can indicate either reaction with

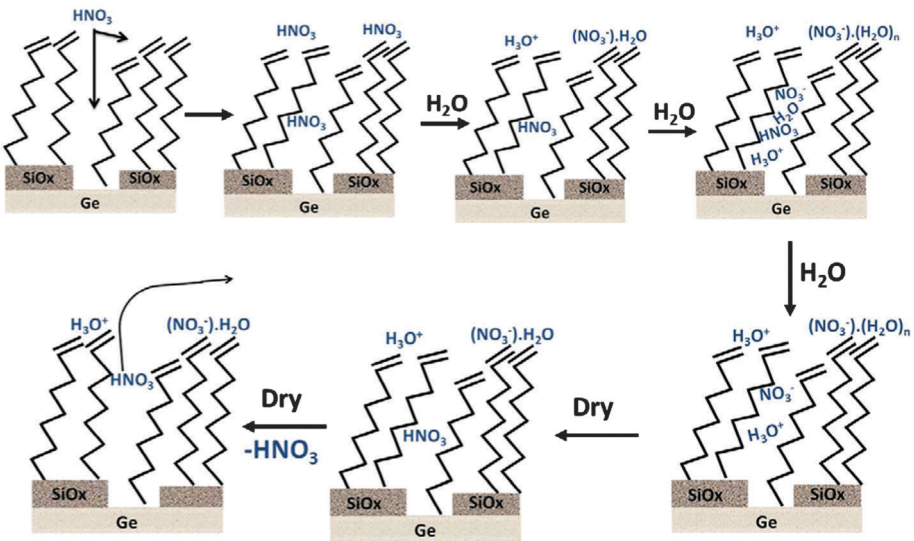

Fig. 6 Schematic of interaction of HNO_3 and H_2O with a C8= SAM.

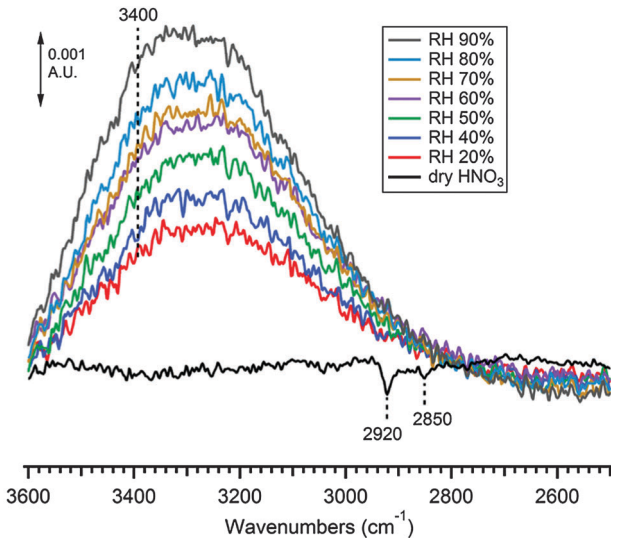

Fig. 7 Infrared spectra of a SiO_x/Ge ATR crystal coated with a C8= SAM in equilibrium with water vapor at 20–90% RH in the absence of HNO_3. For comparison, the black trace is the spectrum on exposure to dry HNO_3.

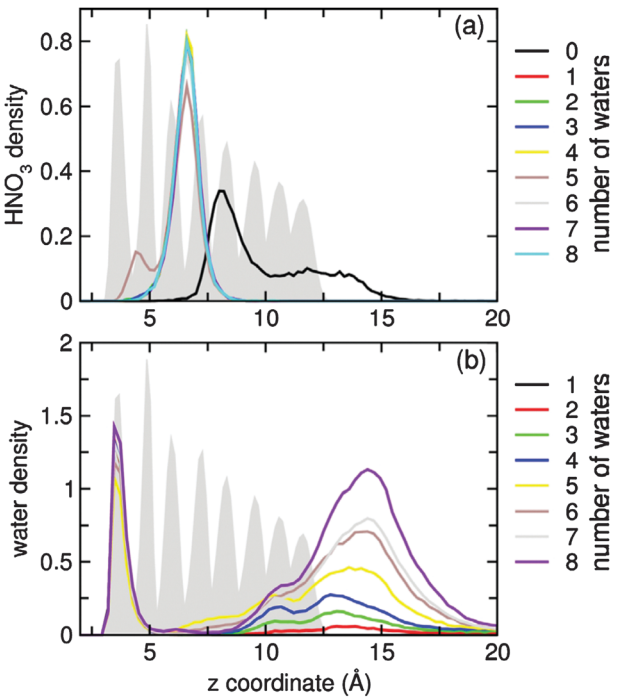

Fig. 8 (a) HNO_3 and (b) water density profiles along the vector normal to the surface (distance z from the substrate) for the four defect simulation with the indicated number of water molecules added. The density profiles are normalized to the number of molecules present in the simulation. The (un-normalized) density profile of the carbon atoms is shown in grey for reference. Note that in (a), the density profiles corresponding to n = 1, 2, 3, 4, 6, 7, 8 are nearly indistinguishable.

removal of some of the SAM, or increased disorder[54,55,102,103,106] in the organic monolayer. Although it is possible that HNO_3 reacts with the unsaturated portion of the SAM, peaks due to expected reaction products (*e.g.*, organic nitrates or carbonyl-containing compounds) were never observed in the IR spectra. However, decreases in the ν_{as} and ν_s stretches[45,54,55,59] of $-CH_2-$ at 2920 and 2850 cm^{-1} were observed when the SAM-coated crystal was exposed to HNO_3 either dry or after the addition of water (Fig. 4); as seen in Fig. 7, such decreases did not occur upon exposure to water in the absence of HNO_3. In addition, upon drying overnight where the molecular HNO_3 has been removed (Fig. 5), the spectra in the $-CH_2-$ stretching region revert to that of the unperturbed SAM prior to exposure to HNO_3. This is consistent with HNO_3 penetrating into the SAM, causing a disordering of the monolayer. The fact that HNO_3 intercalates in this manner is consistent with the reported interactions of HNO_3 with CCl_4[43] and with condensed phase organics,[4] and with the recent proposal that undissociated HNO_3 interacts weakly with water.[33,34]

C. Molecular dynamics simulations of the interaction of gaseous HNO_3 and water vapor with a self-assembled monolayer

Fig. 8 shows density profiles of HNO_3 and water (if present) as a function of distance (z) away from the substrate. Relative density profiles for carbon are also shown, from which the point of separation between the gas phase and the SAM can be seen to occur at 12.5 Å.

Upon exposure of the defective self-assembled monolayer to HNO_3 with no water present, nitric acid preferentially resides in the pockets of the monolayer formed by the defects. However, it is prevented from interacting directly with the substrate by SAM molecules which adopt arrangements which protect the defect (Fig. 8a, black line). However, after water vapor is introduced into the simulation cell, the formation of a water–HNO_3 dimer is observed that resides deep in the monolayer. The water–HNO_3 dimer, formed *via* a hydrogen bond involving the acidic proton, is consistently oriented such that the coordinating water is buried deepest, followed by HNO_3 which has its proton pointed toward the oxygen of the water. The arrangement of the water–HNO_3 dimer can be clearly seen in the density profiles shown in Fig. 8 where the sharp peaks in Fig. 8b at ~4 Å correspond to a single water and the associated HNO_3 peaks are observed at ~7 Å in Fig. 8a. Calculation of the radial distribution functions (not shown) between the proton and oxygen of water verifies that the hydrogen bond of the dimer is persistent over the course of the simulation, an indication that the dimer is highly stable. Shown in Fig. 9 is a representative snapshot taken from simulation of the water–HNO_3 dimer buried in the monolayer. From the snapshot in side-view Fig. 9a, HNO_3 can be seen to reside in a protective pocket of the monolayer, with its proton pointing away from the gas phase. The snapshot in the top-view in Fig. 9b shows the hydrocarbon chain in an arrangement which encapsulates the HNO_3.

Although the model of nitric acid does not permit dissociation, we hypothesize that molecular HNO_3 could be stabilized in the defect. Our simulations suggest the dimer is oriented such that the acidic proton of HNO_3 is pointing away from the gas phase and therefore unable to interact with the minimum number of water molecules needed to stabilize the contact ion pair.[9–11]

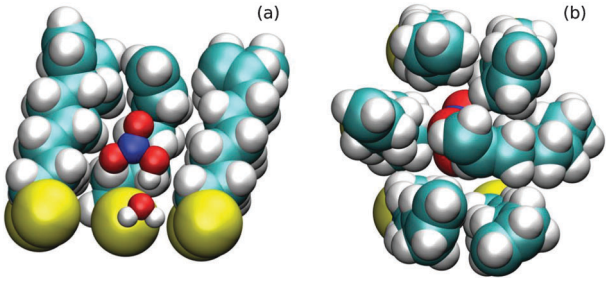

Fig. 9 Representative snapshots taken from the simulations that represent the most probable configuration when any water is present. A side view is shown in (a) and a top view in (b). The atoms are colored as follows: sulfur (yellow), carbon (cyan), oxygen (red), nitrogen (blue), and hydrogen (white). For clarity, only the nearest 5 (a) or 6 (b) alkylthiols are shown.

The simulations indicate that HNO_3 interacts directly with only one isolated water molecule and only sparingly with the remaining water molecules present in the gas phase. It is important to note that although we speculate here that dissociation is unlikely to occur in the defect configuration modeled, this does not preclude the possibility that chemistry may occur with the siloxanes, or that variations in defect size and shape may stabilize contact ion pairs. Indeed, our simulations of other defect sizes and shapes exhibit some variations in the density profiles of both sequestered HNO_3 and water.

There is additional support for the role of the SAM in trapping HNO_3 under dry conditions and preventing it from interacting with water vapor. In an experiment in which the SAM was exposed directly to a mixture of HNO_3 and H_2O corresponding to 50% RH, only the formation of nitrate ions on the surface was observed; there was no evidence of molecular HNO_3 on the surface. Under these conditions, water is readily available when HNO_3 is taken up on the surface and dissociation to NO_3^- and H_3O^+ occurs immediately. No change in the $-CH_2-$ stretch absorptions was observed in this case, indicating the SAM was not further perturbed as was the case when dry HNO_3 was introduced. This suggests that the combination of nitric acid and water leads to rapid dissociation on the surface of the SAM, before HNO_3 can penetrate into the film.

Atmospheric implications

In the troposphere, organic thin films are common on surfaces in the boundary layer[38–42] and on airborne particles.[1] These coexist with gas phase nitric acid formed *via* NO_x oxidation.[1] Water vapor is also present in significant concentrations, even in relatively dry environments (*e.g.* deserts). Thus, it is likely that the simultaneous deposition of nitric acid and water on organic-coated surfaces or on particles will lead to rapid dissociation of the acid on the surface, rather than migration into the film where it could be trapped as molecular HNO_3. In this case, the chemistry and photochemistry of deposited HNO_3 will be dominated by that of the nitrate ion, rather than molecular HNO_3. (Note, however, that hydrates of molecular HNO_3 were observed from the hydrolysis of NO_2 in earlier studies on silica surfaces[25] which suggests they could play a role in the absence of organic coatings.) There is evidence that the photochemistry of the nitrate ions formed on surfaces may differ from that in bulk aqueous solutions. Thus, the quantum yields for photolysis are larger when the ion is at the interface of aqueous solutions where there is an incomplete solvent cage.[107–116] The production of OH radicals *via* the well known photochemistry in bulk aqueous solutions[117,118]

$$NO_3^- + h\nu \rightarrow NO_2 + O^- \quad (3)$$

$$\rightarrow NO_2^- + O(^3P) \quad (4)$$

$$O^- + H_2O \rightarrow OH + HO^- \quad (5)$$

could therefore lead to more efficient oxidation of the surface. On the other hand, one might expect efficient recombination of the photo-fragments of nitrate ions trapped within the SAM, leading to smaller effective quantum yields and less oxidation initiated along the chains. The composition of urban surface films is a complex mixture of organic compounds ranging from short chain aliphatics to long chain fatty acids,[42] and as a result, will be more disordered than a SAM. A more disordered film will have more pores and pockets that allow gases to more readily penetrate the film and be trapped there, increasing the efficiency of recombination of the photo-fragments of nitrate ions and hence trapping of nitric acid molecules.

There may be cases where HNO_3 is formed inside an organic film and hence contribute to the chemistry and photochemistry, along with nitrate ions. For example, ozone,[119] and likely NO_2, can be trapped in organic media. Reaction between NO_2 and O_3 forms the nitrate radical which readily abstracts hydrogen atoms from organics to form HNO_3.[1] Similarly, uptake and hydrolysis of NO_2 and N_2O_5 form HNO_3;[1,94] there may be circumstances where there is sufficient water associated with the organic film for the hydrolysis to occur, but not enough to dissociate the HNO_3 product. While the photolysis of nitrate ions is reasonably well understood,[117,118] that of adsorbed nitric acid is less certain. Zhu and coworkers,[120–123] for example, report that the absorption cross sections and quantum yields for nitric acid photolysis adsorbed on inorganic surfaces such as silica are much larger than in the gas phase. Whether the same is true for nitric acid on or in an organic film remains to be investigated. Efficient recombination of the initially formed fragments trapped inside a defect/pocket of the organic layer could provide a counter-balancing effect that leads to less, rather than more, efficient photochemistry compared to the gas phase.

Acknowledgements

The authors wish to acknowledge the use of the facilities at the Carl Zeiss Center for Excellence in Electron Microscopy at the University of California, Irvine. The authors would also like to thank Mark Bachman and Ruisheng Chang from the Integrated Nano Research Facility (INRF) at the University of California, Irvine for the PEVCD coating of the crystal. S.G.M. would like to thank the Air & Waste Management Association (AWMA) for a scholarship and the Michael E. Gebel Award Fund for partial

financial support. J.D.R. is grateful to the National Science Foundation for fellowship support under CHE-0836070. Helpful discussions with R. Benny Gerber, John Hemminger, Sergey Nizkorodov, Theresa McIntire and John Porter are gratefully acknowledged, as are discussions and comments on the manuscript by James N. Pitts Jr. This work was carried out at AirUCI, an Environmental Molecular Sciences Institute funded by the National Science Foundation (Grant # CHE-0431312 and 0909227).

References

1 B. J. Finlayson-Pitts and J. N. Pitts, *Chemistry of the Upper and Lower Atmosphere: Theory, Experiments and Applications*, Academic Press, San Diego, 2000.
2 X. L. Zhou, H. L. Gao, Y. He, G. Huang, S. B. Bertman, K. Civerolo and J. Schwab, *Geophys. Res. Lett.*, 2003, **30**, DOI: 10.1029/2003GL018620.
3 X. L. Zhou, Y. He, G. Huang, T. D. Thornberry, M. A. Carroll and S. B. Bertman, *Geophys. Res. Lett.*, 2002, **29**, DOI: 10.1029/2002GL015080.
4 S. R. Handley, D. Clifford and D. J. Donaldson, *Environ. Sci. Technol.*, 2007, **41**, 3898.
5 M. Mochida and B. J. Finlayson-Pitts, *J. Phys. Chem. A*, 2000, **104**, 9705.
6 A. M. Rivera-Figueroa, A. L. Sumner and B. J. Finlayson-Pitts, *Environ. Sci. Technol.*, 2003, **37**, 548.
7 N. A. Saliba, H. Yang and B. J. Finlayson-Pitts, *J. Phys. Chem. A*, 2001, **105**, 10339.
8 L. D. Ziemba, J. E. Dibb, R. J. Griffin, C. H. Anderson, S. I. Whitlow, B. L. Lefer, B. Rappenglück and J. Flynn, *Atmos. Environ.*, 2010, **44**, 4081.
9 X. Zhang, E. L. Mereand and A. W. Castleman, *J. Phys. Chem.*, 1994, **98**, 3554.
10 B. D. Kay, V. Hermann and A. W. Castleman, *Chem. Phys. Lett.*, 1981, **80**, 469.
11 J. J. Gilligan and A. W. Castleman, *J. Phys. Chem. A*, 2001, **105**, 5601.
12 E. Högfeldt, *Acta Chem. Scand.*, 1963, **17**, 785.
13 J. P. D. Abbatt, *Geophys. Res. Lett.*, 1997, **24**, 1479.
14 P. K. Hudson, J. E. Shilling, M. A. Tolbert and O. B. Toon, *J. Phys. Chem. A*, 2002, **106**, 9874.
15 L. F. Keyser and M. T. Leu, *Microsc. Res. Tech.*, 1993, **25**, 434.
16 O. Mohler, H. Bunz and O. Stetzer, *Atmos. Chem. Phys.*, 2006, **6**, 3035.
17 I. K. Ortega, B. Mate, M. A. Moreno, V. J. Herrero and R. Escribano, *Geophys. Res. Lett.*, 2006, **33**, L19816.
18 S. Peil, S. Seisel and O. Schrems, *J. Mol. Struct.*, 1995, **348**, 449.
19 M. Sato, O. Setokuchi, K. M. T. Yamada and T. Ibusuki, *Vib. Spectrosc.*, 2003, **31**, 167.
20 O. Stetzer, O. Mohler, R. Wagner, S. Benz, H. Saathoff, H. Bunz and O. Indris, *Atmos. Chem. Phys.*, 2006, **6**, 3023.
21 R. T. Tisdale, A. J. Prenni, L. T. Iraci, M. A. Tolbert and O. B. Toon, *Geophys. Res. Lett.*, 1999, **26**, 707.
22 M. A. Tolbert and A. M. Middlebrook, *J. Geophys. Res.*, 1991, **95**, 22423.
23 G. Ritzhaupt and J. P. Devlin, *J. Phys. Chem.*, 1991, **95**, 90.
24 P. R. McCurdy, W. P. Hess and S. S. Xantheas, *J. Phys. Chem. A*, 2002, **106**, 7628.
25 K. A. Ramazan, L. M. Wingen, Y. Miller, G. M. Chaban, R. B. Gerber, S. S. Xantheas and B. J. Finlayson-Pitts, *J. Phys. Chem. A*, 2006, **110**, 6886.
26 H. Yang and B. J. Finlayson-Pitts, *J. Phys. Chem. A*, 2001, **105**, 1890.
27 R. Bianco, S. Z. Wang and J. T. Hynes, *J. Phys. Chem. A*, 2007, **111**, 11033.
28 S. Z. Wang, R. Bianco and J. T. Hynes, *J. Phys. Chem. A*, 2009, **113**, 1295.
29 M. C. K. Soule, P. G. Blower and G. L. Richmond, *J. Phys. Chem. A*, 2007, **111**, 3349.
30 E. S. Shamay, V. Buch, M. Parrinello and G. L. Richmond, *J. Am. Chem. Soc.*, 2007, **129**, 12910.
31 C. Schnitzer, S. Baldelli, D. J. Campbell and M. J. Shultz, *J. Phys. Chem. A*, 1999, **103**, 6383.
32 M. J. Shultz, C. Schnitzer, D. Simonelli and S. Baldelli, *Int. Rev. Phys. Chem.*, 2000, **19**, 123.
33 T. Lewis, B. Winter, A. C. Stern, M. D. Baer, C. J. Mundy, D. J. Tobias and J. C. Hemminger, *J. Phys. Chem. C*, 2011, **115**, 21183.
34 T. Lewis, B. Winter, A. C. Stern, M. D. Baer, C. J. Mundy, D. J. Tobias and J. C. Hemminger, *J. Phys. Chem. B*, 2012, **115**, 9445.
35 G. E. Ewing, *J. Phys. Chem. B*, 2004, **108**, 15953.
36 G. E. Ewing, *Chem. Rev.*, 2006, **106**, 1511.
37 A. L. Sumner, E. J. Menke, Y. Dubowski, J. T. Newberg, R. M. Penner, J. C. Hemminger, L. M. Wingen, T. Brauers and B. J. Finlayson-Pitts, *Phys. Chem. Chem. Phys.*, 2004, **6**, 604.
38 M. L. Diamond, S. E. Gingrich, K. Fertuck, B. E. McCarry, G. A. Stern, B. Billeck, B. Grift, D. Brooker and T. D. Yager, *Environ. Sci. Technol.*, 2000, **34**, 2900.
39 S. E. Gingrich and M. L. Diamond, *Environ. Sci. Technol.*, 2001, **35**, 4031.
40 B. Lam, M. L. Diamond, A. J. Simpson, P. A. Makar, J. Truong and N. A. Hernandez-Martinez, *Atmos. Environ.*, 2005, **39**, 6578.
41 N. L. Law and M. L. Diamond, *Chemosphere*, 1998, **36**, 2607.
42 A. J. Simpson, B. Lam, M. L. Diamond, D. J. Donaldson, B. A. Lefebvre, A. Q. Moser, A. J. Williams, N. I. Larin and M. P. Kvasha, *Chemosphere*, 2006, **63**, 142.
43 M. H. Kuo, A. David, N. Kamelamela, M. White and M. J. Shultz, *J. Phys. Chem. C*, 2007, **111**, 8827.
44 N. J. Harrick, *Internal Reflection Spectroscopy*, Wiley Interscience Publishers, New York, 1967.
45 Y. Dubowski, J. Vieceli, D. J. Tobias, A. Gomez, A. Lin, S. A. Nizkorodov, T. M. McIntire and B. J. Finlayson-Pitts, *J. Phys. Chem. A*, 2004, **108**, 10473.
46 T. M. McIntire, A. S. Lea, D. J. Gaspar, N. Jaitly, Y. Dubowski, Q. Q. Li and B. J. Finlayson-Pitts, *Phys. Chem. Chem. Phys.*, 2005, **7**, 3605.
47 T. M. McIntire, S. R. Smalley, J. T. Newberg, A. S. Lea, J. C. Hemminger and B. J. Finlayson-Pitts, *Langmuir*, 2006, **22**, 5617.
48 L. R. Fiegland, M. M. Saint Fleur and J. R. Morris, *Langmuir*, 2005, **21**, 2660.
49 Y. Rudich, *Chem. Rev.*, 2003, **103**, 5097.
50 E. Thomas, Y. Rudich, S. Trakhtenberg and R. Ussyshkin, *J. Geophys. Res.*, 1999, **104**, 16053.
51 E. R. Thomas, G. J. Frost and Y. Rudich, *J. Geophys. Res.*, 2001, **106**, 3045.
52 A. B. Voges, G. Y. Stokes, J. M. Gibbs-Davis, R. B. Lettan, P. A. Bertin, R. C. Pike, S. T. Nguyen, K. A. Scheidt and F. M. Geiger, *J. Phys. Chem. C*, 2007, **111**, 1567.
53 C. Waring, P. A. J. Bagot, M. W. P. Bebbington, M. T. Raisanen, M. Buck, M. L. Costen and K. G. McKendrick, *J. Phys. Chem. Lett.*, 2010, **1**, 1917.
54 R. Maoz and J. Sagiv, *J. Colloid Interface Sci.*, 1984, **100**, 465.
55 D. L. Angst and G. W. Simmons, *Langmuir*, 1991, **7**, 2236.
56 M. Wang, K. M. Liechti, Q. Wang and J. M. White, *Langmuir*, 2005, **21**, 1848.
57 S. R. Wasserman, Y. T. Tao and G. M. Whitesides, *Langmuir*, 1989, **5**, 1074.
58 G. M. Whitesides and P. E. Laibinis, *Langmuir*, 1990, **6**, 87.
59 S. G. Moussa, T. M. McIntire, M. Szori, M. Roeselova, D. J. Tobias, R. L. Grimm, J. C. Hemminger and B. J. Finlayson-Pitts, *J. Phys. Chem. A*, 2009, **113**, 2060.
60 S. G. Moussa and B. J. Finlayson-Pitts, *Phys. Chem. Chem. Phys.*, 2010, **12**, 9419.
61 K. S. Carslaw, S. L. Clegg and P. Brimblecombe, *J. Phys. Chem.*, 1995, **99**, 11557.
62 I. N. Tang, H. R. Munkelwitz and J. H. Lee, *Atmos. Environ.*, 1988, **22**, 2579.
63 W. Mar and M. L. Klein, *Langmuir*, 1994, **10**, 188.
64 H. Yamamoto, T. Watanabe and I. Ohdomari, *J. Chem. Phys.*, 2008, **128**, 164710.
65 D. L. Allara, A. N. Parikh and F. Rondelez, *Langmuir*, 1995, **11**, 2357.
66 M. D. Porter, T. B. Bright, D. L. Allara and C. E. D. Chidsey, *J. Am. Chem. Soc.*, 1987, **109**, 3559.
67 A. Ulman, *Chem. Rev.*, 1996, **96**, 1533.
68 M. Tarek, K. Tu, D. J. Tobias and M. L. Klein, *Biophys. J.*, 1999, **77**, 964.
69 M. Baaden, M. Burgard and G. J. Wipff, *J. Phys. Chem. B*, 2001, **105**, 11131.

70 W. J. Jorgensen, J. Chandrasekhar, J. Madura, R. Impey and M. L. Klein, *J. Chem. Phys.*, 1983, **79**, 926.
71 H. Grubmuller, H. Heller, A. Windemuth and K. Schulten, *Mol. Simul.*, 1991, **6**, 121.
72 U. Essmann, L. Perera, M. L. Berkowitz, T. Darden, H. Lee and L. G. Pedersen, *J. Chem. Phys.*, 1995, **103**, 8577.
73 J. C. Phillips, R. Braun, W. Wang, J. Gumbart, E. Tajkhorshid, E. Villa, C. Chipot, R. D. Skeel, L. Kale and K. Schulten, *J. Comput. Chem.*, 2005, **26**, 1781.
74 M. R. Querry and I. L. Tyler, *J. Chem. Phys.*, 1980, **72**, 2495.
75 U. M. Biermann, B. P. Luo and T. Peter, *J. Phys. Chem. A*, 2000, **104**, 783.
76 G. E. McGraw, D. L. Bernitt and I. Hisatsune, *J. Chem. Phys.*, 1965, **42**, 237.
77 H. Cohn, C. K. Ingold and H. G. Poole, *J. Chem. Soc.*, 1952, 4272.
78 S. E. Anthony, T. B. Onasch, R. T. Tisdale, R. S. Disselkamp, M. A. Tolbert and J. C. Wilson, *J. Geophys. Res.*, 1997, **102**, 10777.
79 R. H. Smith, M. T. Leu and L. F. Keyser, *J. Phys. Chem.*, 1991, **95**, 5924.
80 G. Socrates, *Infrared and Raman characteristic group frequencies*, John Wiley & Sons Ltd, 2001.
81 G. M. Underwood, T. M. Miller and V. H. Grassian, *J. Phys. Chem. A*, 1999, **103**, 6184.
82 D. E. Bethell and N. Sheppard, *J. Chem. Phys.*, 1953, **21**, 1421.
83 C. D. Mashburn, E. K. Frinak and M. A. Tolbert, *J. Geophys. Res.*, 2006, **111**, D15213.
84 J. Baltrusaitis, J. Schuttlefield, J. H. Jensen and V. H. Grassian, *Phys. Chem. Chem. Phys.*, 2007, **9**, 4970.
85 X. B. Wang, X. Yang and L. S. Wang, *J. Chem. Phys.*, 2002, **116**, 561.
86 R. Bianco, S. Z. Wang and J. T. Hynes, *J. Phys. Chem. A*, 2008, **112**, 9467.
87 D. J. Goebbert, E. Garand, T. Wende, R. Bergmann, G. Meijer, K. R. Asmis and D. M. Neumark, *J. Phys. Chem. A*, 2009, **113**, 7584.
88 R. Vogt and B. J. Finlayson-Pitts, *J. Phys. Chem.*, 1994, **98**, 3747.
89 W. S. Barney and B. J. Finlayson-Pitts, *J. Phys. Chem. A*, 2000, **104**, 171.
90 A. L. Goodman, E. T. Bernard and V. H. Grassian, *J. Phys. Chem. A*, 2001, **105**, 6443.
91 M. C. Cretella and H. C. Gatos, *J. Electrochem. Soc.*, 1958, **105**, 487.
92 E. W. Valyocsik, *J. Electrochem. Soc.*, 1967, **114**, 176.
93 F. L. Edelman, L. N. Alexandrov, L. I. Fedina and V. S. Latuta, *Thin Solid Films*, 1976, **34**, 107.
94 B. J. Finlayson-Pitts, L. M. Wingen, A. L. Sumner, D. Syomin and K. A. Ramazan, *Phys. Chem. Chem. Phys.*, 2003, **5**, 223.
95 S. S. Cheng, D. A. Scherson and C. N. Sukenik, *J. Am. Chem. Soc.*, 1992, **114**, 5436.
96 J. Matijašević, N. Hassler, G. Reiter and U. P. Fringeli, *Langmuir*, 2008, **24**, 2588.
97 I. C. Stefan and D. A. Scherson, *Langmuir*, 2000, **16**, 5945.
98 J. M. Buriak, *Chem. Rev.*, 2002, **102**, 1271.
99 S. Devouge, J. Conti, A. Goldsztein, E. Gosselin, A. Brans, M. Voué, J. De Coninck, F. Homblé, E. Goormaghtigh and J. Marchand-Brynaert, *J. Colloid Interface Sci.*, 2009, **332**, 408.
100 P. W. Hoffmann, M. Stelzle and J. F. Rabolt, *Langmuir*, 1997, **13**, 1877.
101 O. P. Drugoveiko, K. K. Evstropev, B. S. Kondrateva, Y. A. Petrov and A. M. Shevyakov, *Zh. Prikl. Spektrosk.*, 1975, **22**, 256.
102 J. Sagiv, *J. Am. Chem. Soc.*, 1980, **102**, 92.
103 Q. Zhang, Q. Zhang and L. A. Archer, *J. Phys. Chem. B*, 2006, **110**, 4924.
104 M. Staikova and D. J. Donaldson, *Phys. Chem. Chem. Phys.*, 2001, **3**, 1999.
105 T. J. Lee and J. E. Rice, *J. Phys. Chem.*, 1992, **96**, 650.
106 C. Waring, P. A. J. Bagot, M. T. Räisänen, M. L. Costen and K. G. McKendrick, *J. Phys. Chem. A*, 2009, **113**, 4320.
107 A. Furlan, *J. Phys. Chem. B*, 1999, **103**, 1550.
108 J. D. Graham, J. T. Roberts, L. D. Anderson and V. H. Grassian, *J. Phys. Chem.*, 1996, **100**, 19551.
109 J. Vieceli, I. Chorny and I. Benjamin, *J. Chem. Phys.*, 2001, **115**, 4819.
110 N. Winter and I. Benjamin, *J. Chem. Phys.*, 2004, **121**, 2253.
111 P. Nissenson, C. J. H. Knox, B. J. Finlayson-Pitts, L. F. Phillips and D. Dabdub, *Phys. Chem. Chem. Phys.*, 2006, **8**, 4700.
112 A. Yabushita, T. Hama, D. Iida and M. Kawasaki, *J. Chem. Phys.*, 2008, **129**, DOI: 10.1063/1.2950093.
113 A. Yabushita, D. Iida, T. Hama and M. Kawasaki, *J. Phys Chem. A*, 2008, **112**, 9763.
114 A. Yabushita, N. Kawanaka, M. Kawasaki, P. D. Hamer and D. E. Shallcross, *J. Phys. Chem. A*, 2007, **111**, 8629.
115 L. M. Wingen, A. C. Moskun, S. N. Johnson, J. L. Thomas, M. Roeselova, D. J. Tobias, M. T. Kleinman and B. J. Finlayson-Pitts, *Phys. Chem. Chem. Phys.*, 2008, **10**, 5668.
116 N. K. Richards, L. M. Wingen, K. M. Callahan, N. Nishino, M. T. Kleinman, D. J. Tobias and B. J. Finlayson-Pitts, *J. Phys. Chem. A*, 2011, **115**, 5810.
117 H. Herrmann, *Phys. Chem. Chem. Phys.*, 2007, **9**, 3935.
118 J. Mack and J. R. Bolton, *J. Photochem. Photobiol., A*, 1999, **128**, 1.
119 J. Vieceli, O. L. Ma and D. J. Tobias, *J. Phys. Chem. A*, 2004, **108**, 5806.
120 O. Abida, J. Du and L. Zhu, *Chem. Phys. Lett.*, 2012, **534**, 77.
121 J. Du and L. Zhu, *Chem. Phys. Lett.*, 2011, **511**, 213.
122 C. Z. Zhu, B. Xiang, L. T. Chu and L. Zhu, *J. Phys. Chem. A*, 2010, **114**, 2561.
123 C. Z. Zhu, B. Xiang, L. Zhu and R. Cole, *Chem. Phys. Lett.*, 2008, **458**, 373.

